

# 1 Horizontally transmitted symbiont populations in deep-sea mussels 2 are genetically isolated

3 Devani Romero Picazo<sup>1\*</sup>, Tal Dagan<sup>1</sup>, Rebecca Ansorge<sup>2</sup>, Jillian M. Petersen<sup>3</sup>, Nicole Dubilier<sup>2</sup>,  
4 Anne Kupczok<sup>1\*</sup>

5 <sup>1</sup> Genomic Microbiology Group, Institute of General Microbiology, Christian-Albrechts University,  
6 Kiel

7 <sup>2</sup> Max Planck Institute for Marine Microbiology, Bremen

8 <sup>3</sup> Division of Microbiology and Ecosystem Science, University of Vienna

9 \* Corresponding authors: [dpicazo@ifam.uni-kiel.de](mailto:dpicazo@ifam.uni-kiel.de), [akupczok@ifam.uni-kiel.de](mailto:akupczok@ifam.uni-kiel.de)

10

## 11 Abstract

12 Eukaryotes are habitats for bacterial organisms where the host colonization and dispersal  
13 among individual hosts have consequences for the bacterial ecology and evolution. Vertical  
14 symbiont transmission leads to geographic isolation of the microbial population and  
15 consequently to genetic isolation of microbiotas from individual hosts. In contrast, the extent of  
16 geographic and genetic isolation of horizontally transmitted microbiota is poorly characterized.  
17 Here we show that chemosynthetic symbionts of individual *Bathymodiolus brooksi* mussels  
18 constitute genetically isolated populations. The reconstruction of core genome-wide strain  
19 sequences from high-resolution metagenomes revealed distinct phylogenetic clades. Nucleotide  
20 diversity and strain composition vary along the mussel lifespan and individual hosts show a high  
21 degree of genetic isolation. Our results suggest that the uptake of environmental bacteria is a  
22 restricted process in *B. brooksi*, where self-infection of the gill tissue results in serial founder  
23 effects during symbiont evolution. We conclude that bacterial colonization dynamics over the  
24 host life-cycle is thus an important determinant of population structure and genome evolution of  
25 horizontally transmitted symbionts.

26

27 Bacteria inhabit most eukaryotes where their presence has consequences for key aspects of  
28 their host biology<sup>1</sup>, such as host development<sup>2</sup>, nutrition<sup>3</sup>, or behavior<sup>4</sup>. From the bacterial  
29 perspective, animals constitute an ecological niche, where microbial communities utilize the  
30 resources of their host habitat<sup>5</sup>. The microbiota biodiversity over the host life cycle is determined  
31 by bacteria colonization dynamics and by host properties, including biotic and abiotic factors.  
32 For example, the microbiota can be affected by the host diet<sup>6</sup> or the host physiological state  
33 (e.g., hibernation<sup>7</sup> or pregnancy<sup>8</sup>). In addition, changes in the host environmental conditions  
34 such as temperature<sup>9</sup> or the availability of reduced compounds<sup>10</sup> can have an effect on the  
35 microbiota community composition.

36 Microbiota dispersal over the host life cycle depends on the level of fidelity between the  
37 host and its microbiota; in faithful interactions, vertically transmitted bacteria are transferred  
38 from adults to their progeny during early host developmental stages, while in less faithful  
39 interactions, horizontally transmitted bacteria are acquired from the environment throughout the  
40 host life cycle<sup>11</sup>. Strictly vertically transmitted bacteria are specialized in their host niche and  
41 their association with the host imposes an extreme geographic isolation. Bacterial inheritance  
42 over host generations imposes a strong bottleneck on the microbiota population and leads to  
43 reduced intra-host genetic diversity<sup>12</sup>. Examples are monoclonal or biconal populations  
44 observed in symbiotic bacteria inhabiting grass sharpshooter<sup>13</sup> and pea aphids<sup>14</sup>. Furthermore,  
45 the geographic isolation of vertically transmitted bacteria leads to genetic isolation and to  
46 symbiont genome reduction over time as a consequence of genetic drift<sup>15</sup>. In contrast, dispersal  
47 is expected to be higher for horizontally transmitted bacteria, where host-associated populations  
48 are connected to one another through the environmental pool<sup>16</sup>. Nonetheless, the genetic  
49 diversity of horizontally transmitted microbial populations may also be reduced due to  
50 bottlenecks during symbiont transmission and host colonization. Stochastic effects in the  
51 colonization of horizontally transmitted bacteria may manifest themselves in differences in  
52 microbiota strain composition among hosts<sup>17,18</sup>. This would lead to subdivided symbiont  
53 populations where the geographic isolation of the microbiota depends on the degree of  
54 symbiont dispersal among individual hosts. Geographic isolation of individual hosts over the  
55 host life span would then lead to genetic isolation of the symbiont populations and to symbiont  
56 population structure. Genomic variation and genetic isolation have been observed for  
57 horizontally transmitted symbionts of the human gut microbiome<sup>19</sup> and of the honey bee gut  
58 microbiome<sup>20</sup>. Moreover, structured symbiont populations can also emerge within an individual  
59 host, as observed for *Vibrio fischeri* colonizing the squid light organ, where different light organ

60 crypts are infected by a specific strain<sup>21</sup>. The degree of dispersal of horizontally transmitted  
61 symbionts remains understudied; hence, whether populations from different microbiomes are  
62 intermixing or are genetically isolated is generally unknown.

63 Here we study the microbiota strain composition of horizontally transmitted  
64 endosymbionts across individual *Bathymodiolus brooksi* deep-sea mussels. *Bathymodiolus*  
65 mussels live in a nutritional symbiosis with the chemosynthetic sulfur-oxidizing (SOX) and  
66 methane-oxidizing (MOX) bacteria. The symbionts are acquired horizontally from the seawater  
67 and are harbored in bacteriocytes within the gill epithelium<sup>22,23</sup>. Most *Bathymodiolus* species  
68 harbor only a single 16S rRNA phylotype for each symbiont, including *B. brooksi*<sup>24</sup>.  
69 Nevertheless, a recent metagenomic analysis of *Bathymodiolus* species from hydrothermal  
70 vents in the mid Atlantic ridge showed the presence of different SOX strains with differing  
71 metabolic capacity<sup>25</sup>. Mussel gills constantly develop new filaments that are continuously  
72 infected<sup>26</sup>. However, whether the new gill filaments in *Bathymodiolus brooksi* are colonized  
73 predominantly by environmental bacteria or by symbionts from older filaments of the same host  
74 remains unknown. These two alternative scenarios are expected to impose different degrees of  
75 geographic isolation on the symbiont population: in continuous environmental acquisition, the  
76 level of inter-host dispersal is high while self-infection limits the symbiont dispersal. Here we  
77 studied the impact of tissue colonization dynamics of horizontally transmitted intracellular  
78 symbionts on the degree of symbiont diversity. Furthermore, we quantified the level of genetic  
79 isolation among communities across individual mussels and its impact on symbiont genome  
80 evolution. For that, we implemented a high-resolution metagenomics approach that captures  
81 genome-wide diversity for both symbionts in multiple *Bathymodiolus brooksi* individuals from a  
82 single site.

## 83 **Results**

### 84 *Gene-based metagenomics binning recovers SOX and MOX core genomes*

85 To study the evolution of the SOX and MOX genomes in *Bathymodiolus* mussels we used a  
86 high-resolution metagenomics approach. Twenty-three *B. brooksi* individuals of shell sizes  
87 ranging between 4.8 cm and 24.3 cm were sampled from a single location at a cold seep site in  
88 the northern Gulf of Mexico. Shell size correlates with mussel age<sup>27</sup>; thus, analyzing mussels  
89 within a wide shell size range allowed us to study the symbiont population structure across host  
90 ages. The mussels were sampled from three separate mussel 'clumps' (small mussel patches  
91 residing on the sediment) that were at most 131m apart (Supplementary Fig. 1). Such a 'patchy'

92 distribution has often been observed in deep-sea mussels<sup>28</sup>. To obtain a comprehensive  
93 representation of the bacterial population in individual mussels and to accurately infer strain-  
94 specific genomes, homogenized gill tissue of each mussel was deeply sequenced (on average,  
95 37.8 million paired-end reads of 250bp per sample, Supplementary Table 1). The resulting  
96 metagenomic sequencing data was analyzed by a gene-based binning approach<sup>29</sup>.

97 The prediction of protein-coding genes from the assembled metagenomes yielded a  
98 non-redundant gene catalog of 4.4 million genes that potentially contains every gene present in  
99 the samples. This includes genes from the microbial community and from the mussel host. In  
100 the metagenomics binning step, genes that covary in their abundance across the different  
101 samples were clustered into metagenomic species (MGSs). Our analysis revealed two MGSs  
102 that comprise the SOX and MOX core genomes (Supplementary Fig. 2). The distribution of  
103 gene coverage in individual samples shows that genes in each core genome have a similar  
104 abundance within each mussel. This confirms the classification of the SOX and MOX MGSs as  
105 core genomes. The MOX core genome is the largest MGS and it contains 2,518 genes with a  
106 total length of 1.97 Mbp. A comparison to Gammaproteobacteria marker genes shows that it is  
107 96.2% complete. Furthermore, it contains 1,568 genes (62.3%) that have homologs in MOX-  
108 related genomes. The SOX core genome contains 1,439 genes, has a total length of 1.27 Mbp  
109 and is considered as 80.2% complete. It contains 1,188 genes (82.6%) with homologs in SOX-  
110 related genomes. In addition to the SOX and MOX core genomes, our analysis revealed a third  
111 MGS of 1,449 genes (Supplementary Fig. 2) that was found in low abundance in a single  
112 mussel and, in addition, 98,944 co-abundant gene groups (CAGs, 3-699 genes). Of the 23  
113 metagenomes, four samples were discarded during the metagenomics binning. Two samples  
114 were discarded prior to the binning due to high variance in symbiont marker gene coverages  
115 and two samples were discarded after binning due to low coverage for both symbionts  
116 (Supplementary Figs. 2,3). To gain insight into the SOX and MOX population structure between  
117 hosts, we compared the characteristics of the core genomes across the remaining 19 samples.  
118 The analysis of the core genome coverages shows that SOX is the dominant member of the  
119 mussel microbiota. The differences in the SOX to MOX ratio among the mussel metagenomes  
120 are likely explained by differences in the availability of H<sub>2</sub>S and CH<sub>4</sub> among clumps, which is a  
121 known determinant of SOX and MOX abundance in *Bathymodiolus*<sup>30</sup> (Supplementary  
122 Information, Supplementary Fig. 4).

123 To study symbiont diversity below the species level, we analyzed single nucleotide  
124 variants (SNVs) that were detected in the core genomes of the two symbionts. In this analysis,

125 we considered SNVs that are fixed in a metagenome as well as polymorphic SNVs, i.e., SNVs,  
126 where both the reference and the alternative allele are observed in a single metagenome. We  
127 found 18,070 SNVs in SOX (SNV density of 14 SNVs/kbp, 49 multi-state, 0.27%) and 4,652  
128 SNVs in MOX (SNV density of 2.4 SNVs/kbp, 5 multi-state, 0.11%). The number of polymorphic  
129 SNVs per sample ranges from 162 (0.9%) to 11,064 (61%) for SOX and from 27 (0.58%) to  
130 3,026 (65%) for MOX (Supplementary Table 1), thus, most SNVs are polymorphic in at least  
131 one sample. It is important to note that the observed difference in strain-level diversity between  
132 SOX and MOX cannot be explained by the difference in sequencing depth (Supplementary  
133 Information). These results are in agreement with previous reports of SOX genetic diversity in  
134 other *Bathymodiolus* species<sup>25</sup>. We further revealed that there is genetic diversity in the MOX  
135 symbiont.

136 *Bathymodiolus microbiota* is composed of SOX and MOX strains from several clades.

137 Diversity in natural populations of bacteria is characterized by cohesive associations among  
138 genetic loci that contribute to lineage formation and generate distinguishable genetic clusters  
139 beyond the species level<sup>31</sup>. The formation of niche-specific genotypes (i.e., ecotypes) has been  
140 mainly studied in populations of free-living organisms such as the cyanobacterium  
141 *Prochlorococcus* spp.<sup>32</sup>. Here we consider a strain to be a genetic entity that is present in  
142 multiple hosts and is characterized by a set of clustered variants in the core genome. To study  
143 lineage formation in symbiont populations associated with *Bathymodiolus* mussels, we  
144 reconstructed the strain consensus core genomes from strain-specific variants that show similar  
145 frequencies in a metagenomic sample.

146 The SNVs found in multiple samples and their covariation across samples were used for  
147 strain deconvolution of the core genomes using DESMAN<sup>33</sup>. This revealed that SOX is  
148 composed of eleven different strains with a mean strain core genome sequence identity of  
149 99.52%. Phylogenetic reconstruction shows that the eleven strains cluster into four clades,  
150 which are separated by relatively long internal branches (Fig. 1b). Notably, 849 of the SNVs on  
151 the SOX core genome (4.7%) do not differentiate between strains. Thus, the resulting strain  
152 alignment is invariant for each of these positions and they are termed invariant SNVs from here  
153 on. For MOX, six strains with a mean core genome sequence identity of 99.88% were  
154 reconstructed. The phylogenetic network shows that the six strains cluster into two clades  
155 comprising three strains each (Fig. 1e). Of the total SNVs, 1,138 (24.4%) are invariant in the  
156 strain alignment. The overall MOX branch lengths are shorter than those of SOX. We detected

157 no effect of sequencing coverage on the inference of the strain clades for SOX (Supplementary  
158 Information, Supplementary Fig. 5).

159 To study the community assembly at the strain level, we examined the strain distribution  
160 across individual mussels. Each SOX strain could be identified in between three and eight  
161 samples (frequency  $\geq 5\%$ ; Fig. 1a). Only one or two strains were detected with a frequency of at  
162 least 5% in small mussels ( $\leq 7$  cm), two to nine strains in medium-sized mussels (7.2 cm – 14.1  
163 cm) and one to two strains in large mussels (14.6 cm – 24.1 cm). Notably, only strains from  
164 clades S1 and S2 are present in large mussels ( $\geq 14.6$  cm). One of the large mussels (S) is an  
165 exception as it hosts three SOX strains and contains strains from both clades S1 and S2. Six  
166 mussels have one dominant SOX strain (frequency  $\geq 90\%$ ). Five of these are large mussels (M,  
167 N, P, Q, R) and only one is a small mussel (C). The dominant strain is either S1.4, S2.1, or S2.2  
168 (Fig. 1a; Supplementary Table 1). The MOX strain composition across mussels shows that each  
169 MOX strain occurs (frequency  $\geq 5\%$ ; Fig. 1d) in four to 17 mussels and each mussel contains  
170 two to four MOX strains. Additionally, strains of clade M2 are dominant in ten of the mussels.

171 To investigate the degree of genetic cohesion within strain clades in the population, we  
172 studied the allele frequency spectrum (AFS) of each mussel. A visual inspection of the derived  
173 allele frequency spectra revealed multimodal distributions for both symbiont populations. The  
174 modes reach high allele frequencies and are associated with the main phylogenetic clades; this  
175 suggests that the clades constitute cohesive genetic units (Fig. 1c,f; Supplementary Fig. 6). The  
176 presence of high-frequency modes is especially apparent for SOX in medium-sized mussels  
177 that contain multiple strains. To identify sample-specific strain sequences, we reconstructed  
178 dominant haplotypes (major allele frequency  $\geq 90\%$ ) for the samples that contain a dominant  
179 strain (strain frequency  $\geq 90\%$ ). By comparing dominant haplotypes among samples containing  
180 the same dominant strain, we found that these can contain between 42 and 74 differential SNVs  
181 (Supplementary Table 1). This suggests that the fixation of variants within individual mussels  
182 contributes to the observed population structure.

183 Overall, our results revealed that the symbiont populations are composed of strains that  
184 cluster into few clades, which appear to be maintained by strong cohesive forces. In addition,  
185 the strains are shared among multiple mussels and multiple strains are capable of dominating  
186 different hosts. This suggests that stochastic processes are governing the symbiont community  
187 assembly, as previously proposed for other *Bathymodiolus* species<sup>34</sup>.

188 *SOX strains evolve under purifying selection while MOX evolution is characterized by neutral*  
189 *processes*

190 To study the evolution of SOX and MOX strains in *Bathymodiolus*, we examined the selection  
191 regimes that have been involved in the formation of cohesive genetic SOX and MOX units. The  
192 core genome-wide ratio of pN/pS is higher in MOX (pN/pS of 0.425) in comparison to SOX  
193 (pN/pS of 0.137), which indicates that the strength of purifying selection is higher for SOX. In  
194 addition, we estimated pN/pS for each of the symbiont core genes. This revealed that MOX  
195 genes are characterized by large pN/pS and small pS values, while SOX genes have small  
196 pN/pS and large pS values (Supplementary Fig. 7). The relative rate of nonsynonymous to  
197 synonymous substitutions has been shown to depend on the divergence of the analyzed  
198 species<sup>35,36</sup>. For populations of low divergence, SNVs comprise substitutions that have been  
199 fixed in the population and mutations that arose recently. The latter include slightly deleterious  
200 mutations that were not yet purged by selection, resulting in an elevated ratio of  
201 nonsynonymous to synonymous replacements. Thus, this ratio is not suitable for analyzing  
202 closely related genomes, which is usually the case when studying variation within bacterial  
203 species.

204 To circumvent the bias in pN/pS, we tested for differences in selection regimes in the  
205 evolution of SOX and MOX strains using the neutrality index (NI). NI is used to distinguish  
206 between divergent and polymorphic SNVs and to quantify the departure of a population from the  
207 neutral expectation. An excess of divergent nonsynonymous mutations (NI<1) indicates that the  
208 population underwent positive selection or an important demographic change in the past<sup>37</sup>. We  
209 estimated NI by considering two different levels of divergence and polymorphism. In the first  
210 level, all identified strains are considered as diverged taxonomic units; in the second level, we  
211 disregard the small-scale strain classification and consider only the clades as diverged  
212 taxonomic units (Table 1). Considering all strains as divergent, we observed a low NI<sup>MOX</sup> (<1),  
213 which suggests that MOX evolved under a neutral (NI~1) or positive selection regime. NI<sup>MOX</sup>  
214 increased when considering the clades as diverged, which suggests that the low NI<sup>MOX</sup>  
215 observed at the strain level is the result of an excess of nonsynonymous SNVs within the strain  
216 clades that may constitute transient polymorphisms. Thus, the excess of nonsynonymous  
217 mutations observed for MOX is biased by the low level of divergence; hence, similar to the  
218 pN/pS ratio, it cannot serve as an indication for positive selection. On the other hand, we found  
219 that purifying selection is in action for SOX (NI<sup>SOX</sup>>1). Similar to MOX, when using the clades as

220 divergent,  $NI^{SOX}$  slightly increases. This indicates that the SNVs that differ between clades are  
221 more likely to be substitutions in comparison to those that differ among within-clade strains.

222 Altogether, these results suggest differences in the selection regimes during the  
223 evolution of the SOX and MOX strains. While the SOX core genome is shaped by purifying  
224 selection, we cannot detect deviation from the neutral expectation in the MOX core genome.  
225 These differences likely stem from the different divergence levels among the strains of both  
226 symbiont populations. The association of SOX with *Bathymodiolus* mussels is considered to be  
227 ancient in chemosynthetic deep-sea mussels whereas the MOX association is thought to have  
228 evolved secondarily during *Bathymodiolus* diversification<sup>38</sup>. This is in agreement with the larger  
229 degree of divergence observed here for SOX. Since we observed no evidence for positive  
230 selection on the symbiont core genomes, we suggest that the strains constitute cohesive  
231 genetic units within one ecotype<sup>39</sup>, where all strains are functionally equivalent at the core  
232 genome level. Notwithstanding, the strains might be linked to differences in the accessory gene  
233 content, as observed, for example, in the free-living cyanobacterium *Prochlorococcus* spp.<sup>32</sup> and  
234 in SOX symbionts of other *Bathymodiolus* species<sup>25</sup>.

235 *Intra-sample diversity is higher for SOX than for MOX.*

236 The association with the host limits the dispersal of bacterial populations where the association  
237 across generations is likely maintained by symbiont dispersal between host individuals. If  
238 symbionts are not continuously taken up from the environment, each individual host constitutes  
239 an isolated habitat over its lifetime<sup>5</sup>. Geographic isolation between habitats results in genetic  
240 isolation and contributes to the formation of cohesive associations of genetic loci<sup>31</sup>. Previous  
241 studies showed that geographic isolation during vertical transmission can lead to the reduction  
242 of intra-host genetic diversity in the bacterial populations<sup>12</sup>, nonetheless, the degree of isolation  
243 remains understudied for horizontally transmitted microbes. To characterize the contribution of  
244 geographic isolation to strain formation in the *Bathymodiolous* symbiosis, we next studied the  
245 degree of genetic isolation. Our sample collection of mussels covering a range of sizes (and  
246 thus ages) enabled us to compare symbiont genome diversity among individual hosts of  
247 different age within a single sampling site, thus minimizing the putative effect of biogeography  
248 on population structure. The host species *B. brooksi* is ideal for such an analysis as it grows to  
249 unusually large sizes and possibly lives longer than many other *Bathymodiolus* species. To study  
250 differences in genome diversity of the two symbionts across individual mussels, we estimated



251 the intra-sample nucleotide diversity ( $\pi$ ) and the ecological measure  $\alpha$ -diversity at the resolution  
252 of the SOX and MOX strains.

253 We found a high variability of  $\pi^{\text{SOX}}$  among different mussels (intra-sample  $\pi^{\text{SOX}}$  between  
254  $5.2 \times 10^{-5}$  and  $3.6 \times 10^{-3}$ , Table 2, Fig. 2). Furthermore,  $\pi^{\text{SOX}}$  and the SOX  $\alpha$ -diversity are  
255 significantly positively correlated ( $\rho^2=0.98$ ,  $p < 10^{-6}$ , Spearman correlation, Fig. 2a); hence, the  
256 intra-sample strain diversity is well explained by the nucleotide diversity. The variability in  $\pi^{\text{SOX}}$   
257 agrees with the three age-related groups observed before for the number of SOX strains across  
258 mussel size. Small mussels ( $\leq 7\text{cm}$ ) and large mussels (14.6cm – 24.1cm) have a low  $\pi^{\text{SOX}}$  and  
259 harbor one to two strains. Medium-sized mussels (7.2cm – 14.1cm) have a high  $\pi^{\text{SOX}}$  and harbor  
260 two to nine strains. The community in the largest mussel is an exception, as it has a high  $\pi^{\text{SOX}}$ ,  
261 similar to medium-sized mussels, which can be explained by the presence of three strains from  
262 two clades.

263 The MOX nucleotide diversity is significantly lower in comparison to SOX (intra-sample  
264  $\pi^{\text{MOX}}$  between  $5.6 \times 10^{-6}$  and  $7.0 \times 10^{-4}$ , Table 2, Wilcoxon signed rank test,  $p=0.015$ , Fig. 2).  
265 Similar to SOX, the MOX  $\alpha$ -diversity is significantly positively correlated with  $\pi^{\text{MOX}}$  ( $\rho^2=0.89$ ,  
266  $p < 10^{-6}$ , Spearman correlation) (Fig. 2b). One group of mussels harbors only MOX strains from  
267 clade 2 and is characterized by low MOX nucleotide diversity (A, C, J, L, M, P, Q, R, S,  $\pi^{\text{MOX}}$   
268 between  $5.6 \times 10^{-6}$  and  $2.1 \times 10^{-5}$ ), while the other group harbors MOX strains from both clades and  
269 is characterized by high MOX nucleotide diversity (B, D, E, F, G, H, I, K, N, O,  $\pi^{\text{MOX}}$  between  
270  $1.4 \times 10^{-4}$  and  $7.0 \times 10^{-4}$ ). These groups are not associated with mussel size. Taken together, we  
271 observed a strong correlation between the nucleotide diversity  $\pi$  and  $\alpha$ -diversity for both  
272 symbionts. Notably,  $\pi$  is based on all the detected SNVs whereas the  $\alpha$ -diversity is based only  
273 on the strain composition and relatedness. Thus, the strong correlation demonstrates that the  
274 strain diversity captures most of the core genome-wide nucleotide diversity.

275 A comparison of the  $\pi$  values estimated here to other microbiome studies shows that  
276 higher  $\pi^{\text{SOX}}$  have been observed in other *Bathymodiolus* species (mean between  $2.2 \times 10^{-3}$  and  
277  $3.9 \times 10^{-3}$ )<sup>25</sup>. The average SOX and MOX nucleotide diversity estimated here is within the range  
278 of  $\pi$  values observed in the clam *Solemya velum* microbiome where the symbiont transmission  
279 mode is thought to be a mixture of vertical and horizontal transmission<sup>40</sup>. Furthermore, our  $\pi$   
280 estimates are lower than those observed for most bacterial species in the human gut  
281 microbiome that are considered horizontally transmitted<sup>19</sup>.

282 *Geographic isolation of bacterial communities associated with individual mussels.*

283 Symbiont transmission mode is an important determinant of the community assembly  
284 dynamics<sup>11</sup>. For horizontally transmitted microbiota, similar community composition among  
285 hosts may develop depending on factors that affect the community assembly such as the  
286 environmental bacterial biodiversity or the order of colonization<sup>41</sup>. To study the degree of  
287 geographic isolation between mussel hosts, we calculated genome-wide fixation index  $F_{ST}$  and  
288 the ecological measure  $\beta$ -diversity at the strain resolution across the metagenomic samples for  
289 the two symbionts. Small  $F_{ST}$  indicates that the samples stem from the same population  
290 whereas large  $F_{ST}$  indicates that the samples constitute subpopulations.

291 Our results revealed generally high pairwise  $F_{ST}$  values, indicating a strong genetic  
292 isolation between individual mussels (mean pairwise  $F_{ST}^{SOX}$  of 0.618, mean pairwise  $F_{ST}^{MOX}$  of  
293 0.495, Fig. 2); hence, most mussels in our sample harbor an isolated symbiont subpopulation of  
294 SOX and MOX. In addition, the SOX  $\beta$ -diversity is significantly positively correlated with  
295  $F_{ST}^{SOX}$  ( $\rho^2=0.7$ ,  $p < 10^{-6}$ , Spearman correlation). We observed subpopulations of mussels that are  
296 characterized by a low pairwise  $F_{ST}^{SOX}$  within the subpopulation and a high pairwise  $F_{ST}^{SOX}$  with  
297 other mussels. This subpopulation structure is also represented in the distribution of  $\beta$ -diversity  
298 (Fig. 2). Thus, mussels from the same subpopulation harbor genetically similar SOX  
299 communities and similar strain composition. Examples are one group of mussels including L, O,  
300 P, and Q that contains only strains of clade S2 and another group including the mussels M, N,  
301 and R that contains only strains of clade S1 (Fig. 2a). Notably, the two subpopulations contain  
302 only large mussels that are characterized by a low  $\pi^{SOX}$ .

303 The distribution of pairwise  $F_{ST}^{MOX}$  revealed two main groups: one mussel group is  
304 characterized by high pairwise  $F_{ST}^{MOX}$  and low  $\pi^{MOX}$  while the other group is characterized by  
305 lower  $F_{ST}^{MOX}$  and high  $\pi^{MOX}$  (Fig. 2b). These correspond to the previously described groups,  
306 where one contains mussels with a low  $\pi^{MOX}$  and strains from clade M2 and the other group  
307 contains mussels with a high  $\pi^{MOX}$  and strains from both clades. We did not observe an  
308 association between MOX  $\beta$ -diversity and  $F_{ST}^{MOX}$  ( $p > 0.05$ , Spearman correlation), which can be  
309 explained by the high proportion of invariant SNVs in MOX. Although the analysis of  $F_{ST}^{MOX}$  did  
310 not reveal MOX subpopulations, the pattern of  $\beta$ -diversity uncovered subpopulations that show  
311 a high pairwise  $F_{ST}^{MOX}$ . These subpopulations have a low  $\beta$ -diversity and a low nucleotide  
312 diversity. One subpopulation consisting of large mussels (P, Q, S) is characterized by the

313 presence of strain M2.3 and the absence of clade M1. Another subpopulation (A, C, J, L, M, R)  
314 containing mussels of different sizes is characterized by the dominance of strains M2.1 and  
315 M2.2 and the absence of clade M1. Thus, the comparison of strain composition across mussels  
316 revealed that the population of MOX is substructured similarly to SOX. However, unlike SOX,  
317 the MOX subpopulations are not associated with specific mussel shell sizes.

318 The high  $F_{ST}$  values and the population structure we observed here reveal population  
319 stratification, that is especially pronounced for SOX. One possible factor that influences  
320 symbiont population structure is host genetics, whose impact on the composition of horizontally  
321 transmitted microbiota has been debated in the literature. Studies of the mammal gut  
322 microbiome showed that the host genotype had a contribution to the microbiome composition in  
323 mice<sup>42</sup>, whereas the association with host genetics was reported to be weak in humans<sup>43</sup>.  
324 Analyzing 175 SNVs in 12 mitochondrial genes, we detected no association between mussel  
325  $F_{ST}$  and symbiont  $F_{ST}$  for any of the two symbionts (Supplementary Information, Supplementary  
326 Fig. 8). Consequently, we conclude that the strong subpopulation structure observed for SOX  
327 and MOX cannot be explained by mussel relatedness (i.e., host genetics) or location.

328 Our results provide evidence for a strong genetic isolation between the symbiont  
329 populations associated with individual mussels. This finding is consistent with the observed  
330 individual-specific symbiont strain composition. In contrast, much lower  $F_{ST}$  values were found  
331 for SOX populations in other *Bathymodiolus* species sampled from hydrothermal vents (mean  
332  $F_{ST}$  per site between 0.05 and 0.17), which implies a weaker genetic isolation in these vents<sup>25</sup>.  
333 Our analysis of cold seep *B. brooksi* data revealed SOX subpopulations with low genetic  
334 isolation that are observed using both  $F_{ST}$ , which takes all SNVs into account, and  $\beta$ -diversity at  
335 the level of strains. In contrast, only  $\beta$ -diversity disclosed subpopulations for MOX. Thus, strain-  
336 resolved metagenomics resolves similarities between individual mussel microbiomes below the  
337 species level.

## 338 Discussion

339 Our analysis revealed strong genetic isolation of symbiotic bacterial populations in individual  
340 mussel hosts, indicating geographic isolation between mussels. We hypothesize that this  
341 geographic isolation occurs through restricted uptake of SOX and MOX symbionts from the  
342 environment over time. The lack of evidence for strong adaptive selection in SOX and MOX  
343 strains suggests that the inter-host population structure is the result of neutral processes rather  
344 than host discrimination against different strains. Here, we propose a neutral model for symbiont

345 community assembly that explains how restricted symbiont uptake and colonization impose  
346 barriers to the symbiont dispersal, which can, over time, lead to inter-host population structure  
347 and contribute to the formation of cohesive genetic units within the symbiont population (Fig. 3).  
348 In our model, bacteria are acquired from the environmental symbiont pool in juveniles<sup>44</sup>. The  
349 presence of a symbiont environmental pool was suggested before based on the detection of  
350 symbiont genes in adjacent seawater<sup>45,46</sup>. Nevertheless, the loss of central metabolic enzymes  
351 suggests that bacteria disperse in a dormant state<sup>47</sup>. We hypothesize that the dormancy of free-  
352 living symbionts and the preservation of few symbiont cells inside bacteriocytes<sup>23</sup> contribute to  
353 the isolation of bacterial populations inside the host cells from the rest of the population, which  
354 can lead to recombination barriers. Our results support the self-infection hypothesis<sup>26</sup>, according  
355 to which, once the gill is first colonized, bacteria present in ontogenically older tissue infect  
356 newly formed gill filaments; thus, the uptake of symbionts from the environment is limited. In  
357 addition, decreased growth rate in older mussels may also lead to decreased symbiont uptake.  
358 This model provides a plausible explanation for the observed pattern of strong symbiont genetic  
359 isolation between mussels and of reduced SOX strain diversity in large mussels. Possible later  
360 infections of the gill tissue from the environmental pool may occur due to symbiont loss and  
361 replacement driven by environmental changes or increased gill growth rate. Notably, our results  
362 are in contrast to a recent study on other *Bathymodiolus* species from hydrothermal vents, that  
363 concluded that SOX populations from individual mussels of the same site intermix<sup>25</sup>. This  
364 contrast may be explained by differences in the symbiont abundance in the seawater, which is  
365 expected to play a role in the colonization process. Our samples originate from a cold seep site  
366 with low mussel density (Supplementary Fig. 1); thus, the concentration of symbionts in the  
367 surrounding seawater may be correspondingly low. The low symbiont abundance would result in  
368 a low probability of later infections and a prevalence of self-infection. In contrast, the symbiont  
369 abundance in the seawater at large and densely populated mussel beds at hydrothermal vents  
370 is expected to be higher, resulting in a higher probability of later infections.

371         The colonization of new filaments over the mussel lifespan via self-infection entails serial  
372 founder events on the bacterial population. Throughout this process, new mutations arising in  
373 the symbiont population during the lifetime of the mussel can reach fixation due to genetic drift  
374 following population bottlenecks. This process is expected to lead to a reduction of symbiont  
375 genetic diversity over the mussel life time. Thus, individual mussels develop into independent  
376 habitats that harbor individual populations, which are genetically isolated from other mussel-  
377 associated symbiont populations and from the environmental pool. The evolution of vertically

378 transmitted endosymbiont populations is similarly affected by serial founder effects<sup>48</sup>, as we  
379 suggest here for horizontally transmitted bacteria. However, migration between host-associated  
380 populations and the environmental pool results in an increased effective population size for  
381 horizontally transmitted bacteria; thus, the population is not subject to the fate of genome  
382 degradation as commonly observed in vertically transmitted symbionts<sup>15</sup>. Serial founder effects  
383 and recombination barriers due to geographic isolation are important drivers of lineage  
384 formation in bacteria<sup>39</sup>. Reduction of genetic diversity due to transmission bottlenecks is  
385 considered a hallmark of pathogen genome evolution<sup>49</sup>; examples are *Yersinia pestis*<sup>50</sup> and  
386 *Listeria monocytogenes*<sup>51</sup>. Our model demonstrates that, similar to pathogenic bacteria, genome  
387 evolution of bacteria with a symbiotic lifestyle can be affected by serial founder effects due to  
388 self-infection.

## 389 **Methods**

### 390 *Collection and sequencing*

391 Twenty-three individuals of *Bathymodiolus brooksi* mussels were collected during a research  
392 cruise with the E/V *Nautilus* from the cold seep location GC853 at the northern Gulf of Mexico in  
393 May 2015. The mussel distribution at the cold seep was patchy and mussel individuals were  
394 collected from three distinct clumps within a radius of 131 meters (coordinates clump a:  
395 28.1237, -89.1404 depth: -1073m, clump b: 28.1241, -89.1401 + depth: -1073m, clump c:  
396 28.1237, -89.1404 + depth: -1073 to 1078m). The gills from each mussel individual were  
397 dissected immediately after retrieval and homogenized with sterilized stainless steel beads, 3.2  
398 mm in diameter (biostep, Germany). A subsample of the homogenate for sequencing analyses  
399 was preserved in RNA later (Sigma, Germany) and stored at -80°C. DNA was extracted from  
400 these subsamples as described by<sup>52</sup>. TruSeq library preparation and sequencing using Illumina  
401 HiSeq2500 was performed by the Max Planck Genome Centre in Cologne, Germany, resulting  
402 in 250 bp paired-end reads with a median insert size of 400 bp. The raw reads have been  
403 deposited in NCBI under BioProject PRJNA508280.

### 404 *Construction of the non-redundant gene catalog*

405 Illumina paired-end raw reads from the samples were trimmed for adapters and filtered by  
406 quality using BMap tools<sup>53</sup>. Only reads with more than 30bp and quality above 10 were kept.  
407 This results in 37.7 million paired-end reads per sample on average (Supplementary Table 1).

408 We assembled each of the metagenomic samples individually using metaSPAdes<sup>54</sup>.  
409 Genes were predicted *ab initio* on contigs with metaProdigal<sup>55</sup>. These predicted genes were  
410 clustered by single-linkage according to sequence similarity using BLAT<sup>56</sup> (at least 95% of  
411 sequence identity in at least 90% of the length of the shortest protein and e-value < 10<sup>-6</sup>). To  
412 reduce the potential inflation caused by the single-linkage clustering, we applied two additional  
413 filters to discard hits: the maximum ratio allowed between the two compared sequence lengths  
414 must be 4 and hits between partial and non-partial genes are discarded. These filters are meant  
415 to remove spurious links between sequences due to the presence of commonly spread protein  
416 domains. This clustering was performed in two successive steps; first, we obtained sample-  
417 specific gene catalogs by performing intra-sample clustering. This is meant to reduce sequence  
418 redundancy, resulting in an average of ~676,000 non-redundant genes per sample  
419 (Supplementary Table 1). Second, one-sided similarity search was performed across all pairs of  
420 sample catalogs. This resulted in 1,156,207 clusters (26.5%) and 3,207,869 (73.5%) singletons,  
421 which make up a catalog of 4,364,076 million non-redundant genes. For each of the clusters,  
422 we reconstructed a consensus sequence as cluster representative. To this end, we took the  
423 majority nucleotide at each position (ties were resolved randomly).

#### 424 *Taxonomic annotation of gene catalog*

425 Taxonomic annotation of the gene catalog was performed by aligning the translated genes to  
426 the non-redundant protein NCBI database (date: 24/05/18) using diamond<sup>57</sup> (e-value<10<sup>-3</sup>,  
427 sequence identity ≥ 30%) and obtaining the best hit. Genes were annotated as MOX-related if  
428 their best hit is *Bathymodiolus platifrons* methanotrophic gill symbiont (NCBI Taxonomy ID  
429 113268) or *Methyloprofundus sedimenti* (NCBI Taxonomy ID 1420851). For SOX, the genomes  
430 of thioautotrophic symbionts belonging to four different *Bathymodiolus* species were used for  
431 annotation (NCBI Taxonomy IDs: 2360, 174145, 113267 and 235205). In addition, the gene  
432 catalog was screened for mitochondrial genes using best blastp hits against the *Bathymodiolus*  
433 *platifrons* mitochondrial protein sequences (NC\_035421.1)<sup>58</sup> (all e-values <10<sup>-40</sup>). The gene  
434 catalog was also screened for symbiont marker genes by best blastp hits to a published protein  
435 database for *Bathymodiolus azoricus* symbionts<sup>47</sup> (80% of protein identity and 100% of query  
436 coverage). This allowed to identify 86 SOX and 39 MOX marker genes. The marker gene  
437 coverages are generally uniform across a sample, however a high variance in coverage is  
438 present in two of the samples (Supplementary Fig. 3). Since the binning method relies on the  
439 covariation of coverage across samples, the presence of a high variance in coverage can

440 interfere with the proper clustering of genes, thus, two samples were discarded from further  
441 analysis (Dsc1, Dsc2).

#### 442 *Estimation of the gene catalog coverages*

443 To estimate the gene abundances, we mapped the reads of each metagenomic sample to the  
444 gene catalog using bwa mem<sup>59</sup>. Reads below 95% of sequence identity or mapping quality of  
445 20, as well as not primary alignments were discarded. Coverage per position for each gene in  
446 the catalog across samples was calculated using samtools depth<sup>60</sup> and the gene coverage is  
447 given by the mean coverage across positions. We first downsampled the reads in each sample  
448 to the minimum number of reads found (33M, Supplementary Table 1) and calculated mean  
449 coverage per gene to perform the binning and the analyses of coverage variance across  
450 symbiont marker genes (see above).

#### 451 *Genome binning and symbiont core genome identification*

452 Next, we performed co-abundance gene segregation by using a canopy clustering algorithm<sup>29</sup>,  
453 which clusters genes into bins that covary in their abundances across the different samples.  
454 This approach allows to recover from chimeric associations obtained in the assembly process  
455 and to automatically separate core from accessory genes. Gene coverages across samples  
456 were used as the abundance profiles for binning. First, genes with a Pearson correlation  
457 coefficient (PCC) > 0.9 to the cluster abundance profile were clustered. Then, clusters with PCC  
458 > 0.97 between their median abundance profiles were merged and outlier clusters for which the  
459 coverage signal originates from less than three samples were removed. In addition, we removed  
460 a gene from a cluster if Spearman correlation coefficient to the median canopy coverage profile  
461 is lower than 0.7. Finally, overlaps among the clusters were removed by keeping a gene in the  
462 largest of the clusters in which it has been found.

463 This allowed us to cluster 900,310 genes into 98,944 co-abundant gene groups (3 to 699  
464 genes) and three MetaGenomic Species (MGSs,  $\geq 700$  genes). An additional filter was applied  
465 to the MGSs to obtain final bins by removing outlier genes based on their coverage  
466 (Supplementary Fig. 2). To this end, we used the Median Absolute Deviations (MAD) statistic as  
467 a cutoff to discard highly or lowly covered genes. We removed genes that are at least 24 times  
468 MAD far from the median in at least one of the samples. The bins after outlier gene removal  
469 constitute the core genomes of the MGSs. We checked for the completeness of the symbiont

470 bins with CheckM, by screening for the presence of Gammaproteobacteria universal single copy  
471 marker genes<sup>61</sup>.

#### 472 *SNV discovery on the core genomes*

473 To perform single nucleotide variant (SNV) discovery, we mapped the downsampled reads  
474 individually for each sample to the gene catalog. Because sample size has been shown to have  
475 an effect on variant detection<sup>62</sup>, we normalized the data across samples. To this end, we  
476 normalized each sample to the smallest median coverage found in a sample (482x coverage for  
477 SOX, 36x coverage for MOX and 568x for mitochondrial genes). LoFreq was used for  
478 probabilistic realignment and variant calling of each sample independently<sup>63</sup>. SNVs detected  
479 with LoFreq have been hard filtered using the parameters suggested by GATK best practices<sup>64</sup>.  
480 Briefly, SNVs with quality by depth below 2, Fisher's exact test Phred-scaled probability for  
481 strand bias above 60, root mean square of mapping quality below 40, root mean square of base  
482 quality above 30, mapping quality rank sum test below -12.5 and read position rank sum test  
483 below -8 are kept for further analyses.

484 The resulting SNVs can be fixed or polymorphic in a sample. Polymorphic SNVs are  
485 characterized by the allele frequency of the alternative allele whereas fixed SNVs have an allele  
486 frequency of 1. Here, we define SNVs as polymorphic in a metagenomic sample if their  
487 frequency is between 0.05 and 0.95 in the sample.

#### 488 *Population structure analyses*

489 SNV data is used for calculating intra-sample and inter-sample nucleotide diversity ( $\pi$ ) as  
490 applied before to human gut microbiome species<sup>19</sup>. Intra-sample nucleotide diversity ( $\pi$ ) is given  
491 as:

$$492 \quad \pi(H, G) = \frac{1}{|G|} \sum_{i=1}^{|G|} \sum_{B_1 \in \{ACTG\}} \sum_{B_2 \in \{ACTG\} \setminus B_1} \frac{X_{i,B_1}}{C_i} \frac{X_{i,B_2}}{C_i - 1}$$

493 where  $H$  corresponds to the sample,  $G$  to the bacterial genome,  $|G|$  is the length of the analyzed  
494 genome and  $X_{i,B_j}$  is the count of a specific nucleotide  $B_j$  at a specific locus  $i$  with coverage  $C_i$ .  
495 Inter-sample nucleotide diversity ( $\pi$ ) is then given as follows, where  $H_1$  and  $H_2$  correspond to the  
496 two samples compared:



$$\pi(H_1, H_2, G) = \frac{1}{|G|} \sum_{i=1}^{|G|} \sum_{B_1 \in \{ACTG\}} \sum_{B_2 \in \{ACTG\} \setminus B_1} \frac{X_{i,B_1,S_1}}{C_{i,S_1}} \frac{X_{i,B_2,S_2}}{C_{i,S_2}}$$

498 Finally, these diversity measures are used to estimate the fixation index ( $F_{ST}$ ), which measures  
499 genetic differentiation based on the nucleotide diversity present within and between populations.

$$500 \quad F_{ST}(S_1, S_2, G) = 1 - \frac{\pi_{within}}{\pi_{between}} = 1 - \frac{\pi(S_1, G) + \pi(S_2, G)}{2 \pi(S_1, S_2, G)}$$

501 The scripts to calculate genome-wide inter and intra-sample nucleotide diversity ( $\pi$ ) and fixation  
502 index ( $F_{ST}$ ) across all inter-sample comparisons from pooled SNV data have been deposited at  
503 <https://github.com/deropi/BathyBrooksiSymbionts>.

#### 504 *Strain deconvolution*

505 We reconstructed the strains for the core genomes with DESMAN<sup>33</sup>. The SNVs with two states  
506 and their frequencies in each sample are used by DESMAN to identify strains in the core  
507 genomes that are present over multiple samples. Thereby, the program uses the SNV  
508 frequency covariation across samples to assign the SNV states to a specific genotype. For  
509 SOX, we ran the strain deconvolution five times using different seed numbers and 500  
510 iterations. Due to computational limitations, a subset of 5,000 SNVs was used and the  
511 haplotypes considering the whole SNV dataset were inferred *a posteriori*. The five replicates  
512 were run for an increasing number of strains from seven to twelve. The program uses posterior  
513 mean deviance as a proxy for model fit. A posterior mean deviance lower than 5% was reached  
514 in the transition from eleven to twelve strains, therefore the number of inferred SOX strains is  
515 eleven. We did not run fewer numbers of strains due to the presence of large posterior mean  
516 deviances between runs with a small strain number. Additionally, we ran DESMAN for the SOX  
517 dataset that was subsampled to the MOX coverage with no replicates and eleven strains were  
518 found using posterior mean deviance. For MOX, we ran four replicates using the whole SNV  
519 dataset and 500 iterations. The runs were performed by using an increasing number of strains  
520 from two to seven, reaching the optimal number of six strains. The consensus gene sequences  
521 of each strain were concatenated to generate the strain core genomes, which were used for  
522 further analyses. Splits network of the strain genome sequences were reconstructed using  
523 SplitsTree<sup>65</sup> and uncorrected distances. The position of the root in the splits network was  
524 estimated by the minimum ancestral deviation (MAD) method<sup>66</sup>, which uses maximum likelihood  
525 phylogenetic trees inferred with IQ-TREE<sup>67</sup>.

526 *α- and β-diversity*

527 To study the microbial community composition, we estimated α- and β-diversity accounting for  
528 strain relatedness in addition to species richness and evenness. α-diversity was estimated using  
529 phylogeny species evenness (PSE)<sup>68</sup> implemented in the R package 'Picante'<sup>69</sup>. β-diversity was  
530 estimated using the weighted Unifrac distance, which is implemented in the R package  
531 'GUniFrac'<sup>70</sup>. This measure quantifies differences in strain community composition between two  
532 samples and accounts for phylogenetic relationships.

533 *Allele frequency spectra estimation*

534 The unfolded allele frequency spectra were calculated from biallelic SNVs for each of the  
535 bacterial species within individual samples. The unfolded allele frequency spectrum estimation  
536 relies on the presence of ancestral states in the population. Because we have no information  
537 about the ancestry relationship among the strains present in the samples, we made one main  
538 assumption in this regard: the ancestral SNV state in the population corresponds to the one  
539 which is present in the higher number of strains. Ties are resolved by arbitrarily assigning one  
540 tip of the tree as ancestral state: M2.2 for MOX and S4 for SOX.

541 *pN/pS and Neutrality Index estimation*

542 We estimated pN/pS for both bacterial populations, which is a variant of dN/dS that can be used  
543 based on intra-species SNVs. To this end we first calculated the expected ratio of  
544 nonsynonymous and synonymous mutations for each gene by accounting for each possible  
545 mutation occurring in each of the codons. Then, we estimated the observed nonsynonymous to  
546 synonymous ratio by using the biallelic SNVs. These two measures are later compared,  
547 resulting in the pN/pS ratio. pN/pS was estimated genome-wide as well as individually for each  
548 of the genes in the two symbiont species. The per-gene pN/pS calculation results into  
549 undefined estimates for genes with no synonymous mutations. To circumvent this limitation,  
550 we added 1 to the number of observed synonymous mutations in each gene, which is a  
551 standard correction for dN/dS ratios<sup>71</sup>.

552 The neutrality index (NI) accounts for differences in the ratio of nonsynonymous to  
553 synonymous variants between divergent and polymorphic SNVs in order to quantify the  
554 departure of a population from neutral evolution<sup>37</sup>.  $NI = \frac{pN/pS}{dN/dS}$ , where  $pN$ , and  $pS$  are the  
555 number of polymorphic synonymous and nonsynonymous sites, respectively, and  $dN$  and  $dS$

556 are the number of divergent synonymous and nonsynonymous sites, respectively. For a  
557 coalescent population that evolves neutrally, the nature of fixed mutations that are involved in  
558 the divergence of the strains should not be different from that of the polymorphic mutations. An  
559 excess of divergent nonsynonymous mutations ( $NI < 1$ ) indicates that the population underwent  
560 positive selection or a large demographic change in the past<sup>37</sup>.

561 Here we used the NI to analyze if differences in selection have been involved in the evolution of  
562 SOX and MOX strains. Different strains are typically found in more than one sample and this  
563 supports the notion that SNVs that characterize the strains constitute substitutions. We  
564 estimated NI by considering two different levels of divergence and polymorphism. First, we  
565 defined as divergent all those SNVs that have two possible states among the strains and as  
566 polymorphic all the invariant SNVs. Second, we used a more restrictive level of divergence. To  
567 this end, we excluded putative recently acquired SNVs from the set of divergent SNVs, by  
568 discarding those that have multiple states among strains from the same group. Polymorphic  
569 SNVs are all the remaining. The scripts to calculate the allele frequency spectra, pN/pS and NI  
570 have been deposited at <https://github.com/deropi/BathyBrooksiSymbionts>. Statistics and plotting  
571 were done in R<sup>72</sup>.

## 572 **Acknowledgements**

573 We thank the captain and crew of the E/V *Nautilus* 2015 Expedition, the team of the ROV  
574 *Hercules*, the chief scientist on this expedition leg, Eric Cordes, and the expedition leader, Mike  
575 Brennan. Additionally, we thank Elie Jami, Robin Koch, Tanita Wein, and Christian Wöhle for  
576 critical comments on the manuscript. This work was supported by the CRC1182 *Origin and*  
577 *Function of Metaorganisms*, the Bioinformatics Network at Kiel University, and the North-  
578 German Supercomputing Alliance (HLRN, project shb00002). Additional funding support for ND,  
579 JMP and RA came from the Max Planck Society, the Gordon and Betty Moore Foundation  
580 Marine Microbiology Initiative Investigator Award through grant GBMF3811 to ND and a  
581 European Research Council Advanced Grant (BathyBiome, Grant 340535 to ND).

582

## 583 **Author contributions**

584

585 AK, TD, JMP, and ND designed the study, RA, JMP, and ND collected the data, DRP analyzed

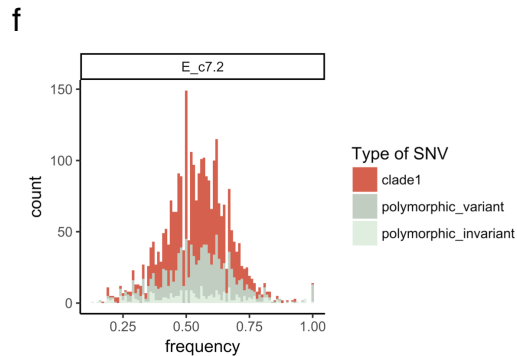
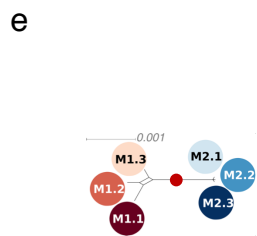
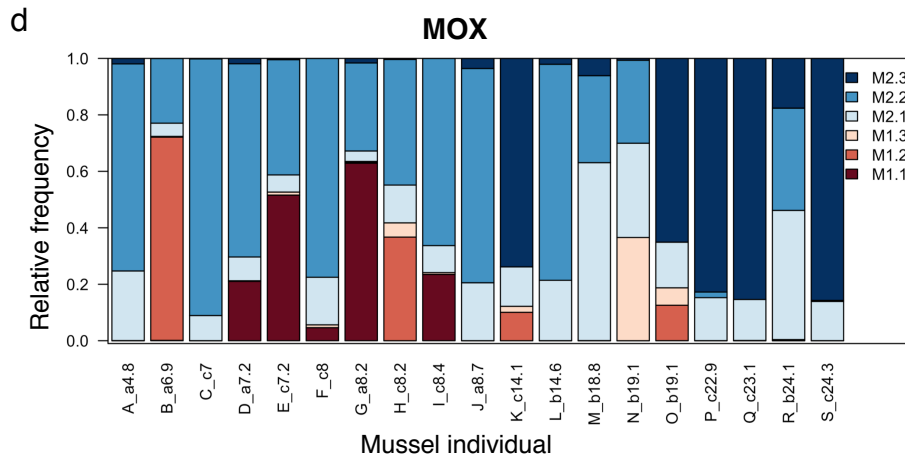
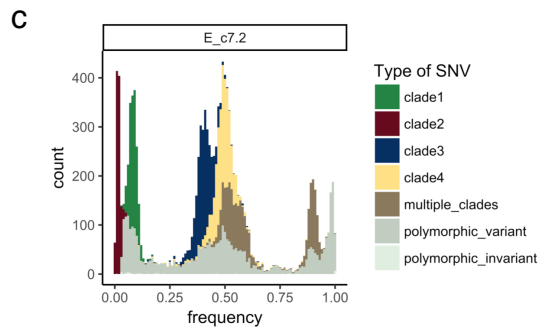
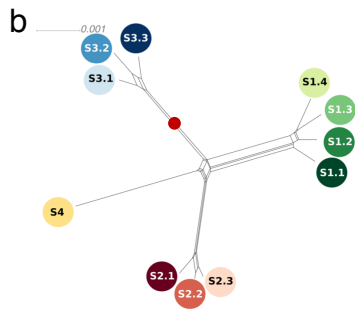
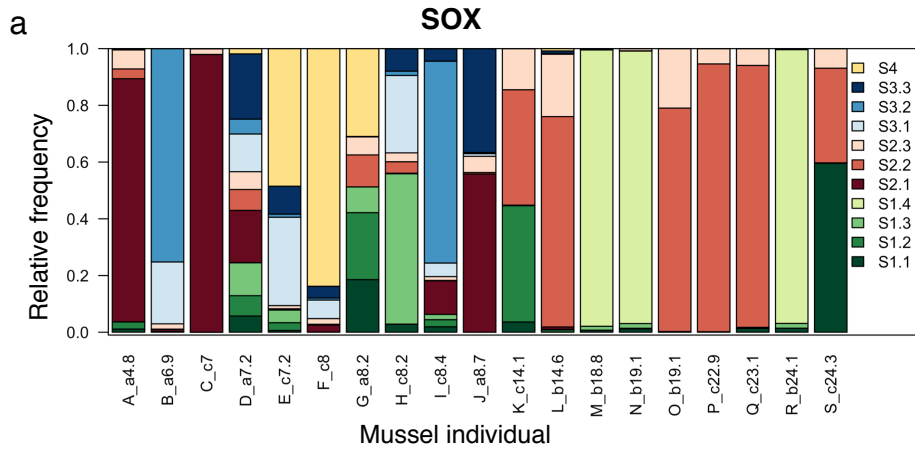
586 the data, DRP, AK, and TD interpreted the results with contribution from RA, DRP, AK, and TD  
587 wrote the manuscript with contributions from all authors.

588

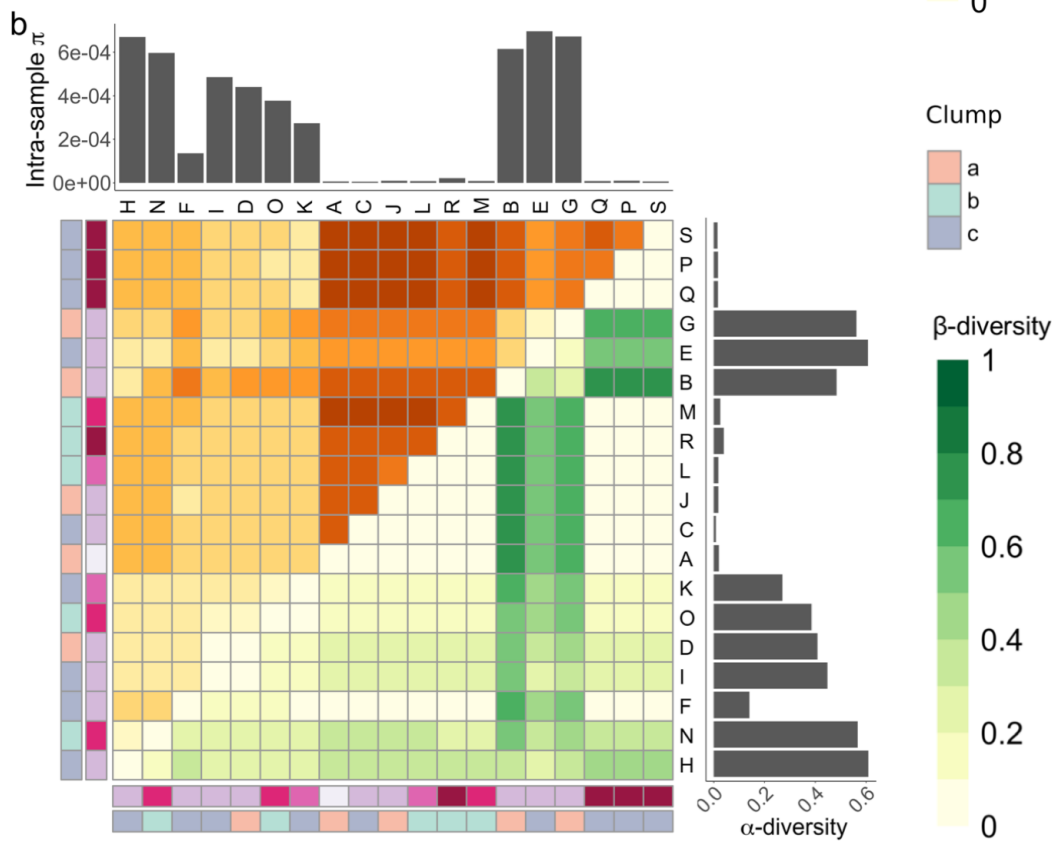
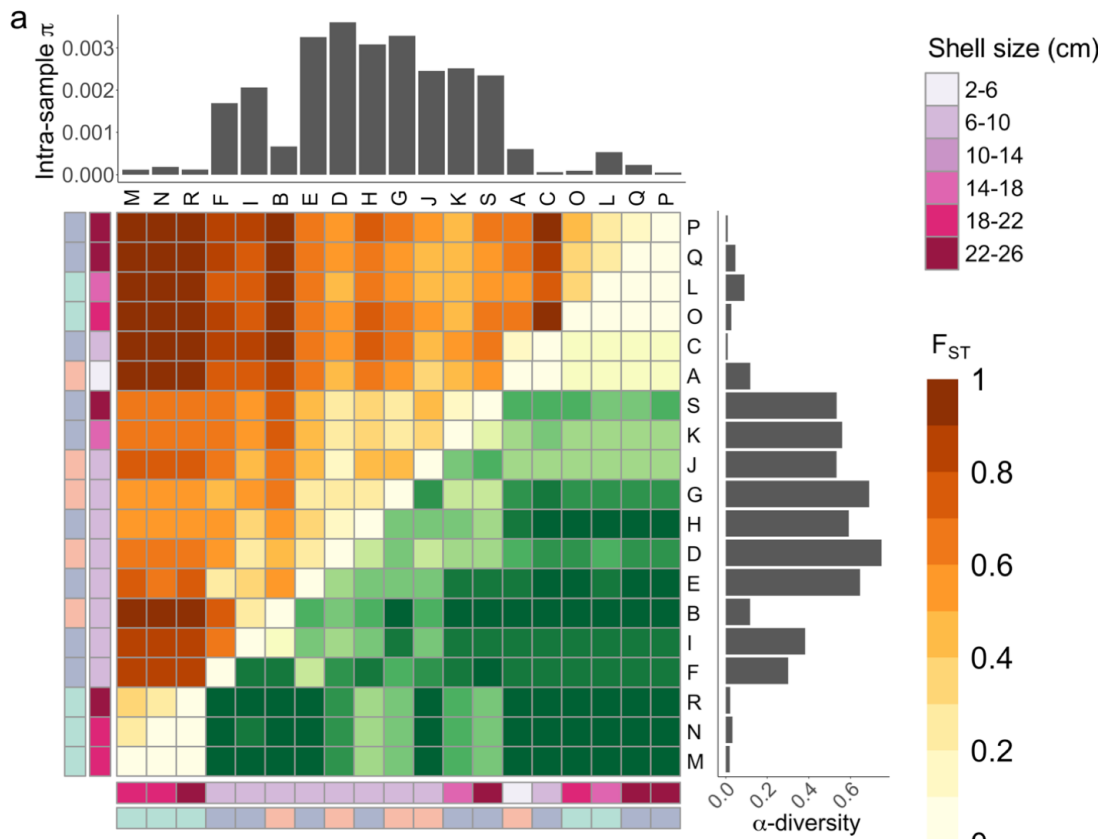
589 **Figure Legends**

590

591



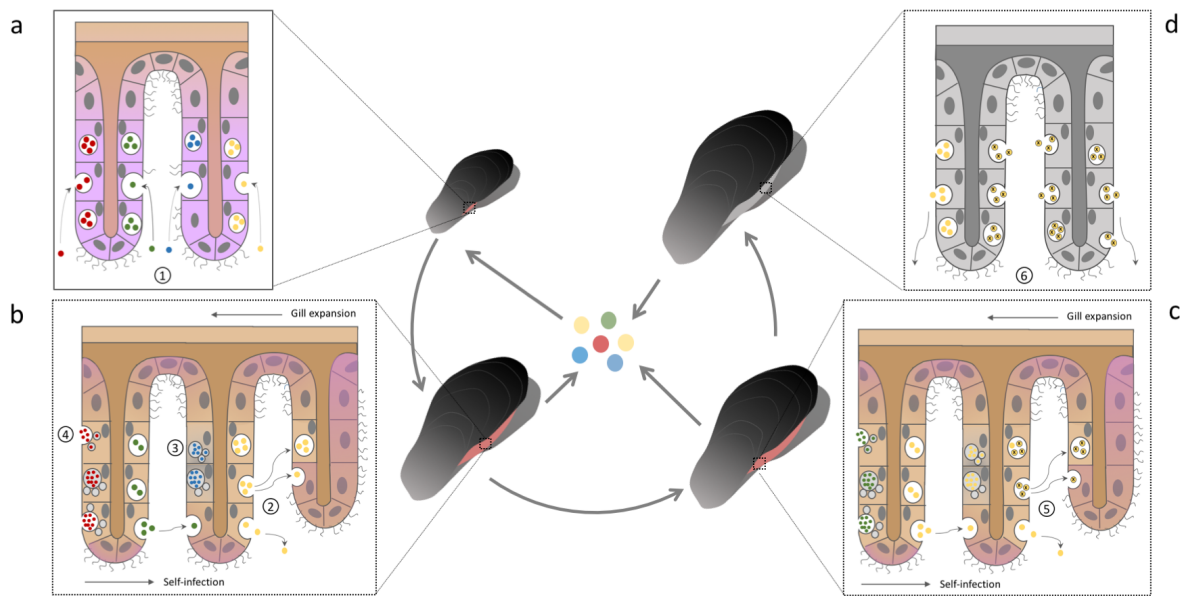
593 **Figure 1: Symbiont strain abundances (a, d), symbiont strain relationships (b, e) and**  
594 **example allele frequency spectra (c, f).** **a, b, c,** 11 strains reconstructed for SOX. These  
595 cluster into four clades, with two times four, three and one strain per clade, labelled by shades  
596 of green, red, blue, and yellow. The strains differ by between 669 SNVs (strains S2.2 and S2.3,  
597 sequence identity 99.95%) and 8,171 SNVs (strains S3.2 and S4 sequence identity 99.36%).  
598 Minimum number of SNVs between strains of different clades is 6,451 (strains S1.1 and S2.1,  
599 sequence identify 99.49%). **d, e, f,** 6 strains reconstructed for MOX. These cluster into two  
600 clades, labelled by shades of red and blue. Strains differ by between 105 (strain M2.2 and M2.3,  
601 sequence identity 99.99%) and 2,677 SNVs (strain M1.1 and M2.1, sequence identity 99.81%).  
602 The minimum number of SNVs differentiating strains from different clades is 2,224 (strains M2.2  
603 and M1.3, sequence identity 99.85%). **a, d,** Stacked barplot of strain relative abundances for  
604 each individual mussel. Mussel individuals are labeled with an assigned letter (A-S), followed by  
605 the sampling clump (a, b or c) and the shell size (cm). **b, e,** Splits network of the strain genome  
606 sequences. Scale bar shows the number of differences per site. The red dots indicate the  
607 position of the root. **c, f,** Example of derived allele frequency spectra (sample E). Different  
608 colors represent different strain clades (see also Supplementary Fig. 6).



610 **Figure 2: Symbiont population structure for a, SOX and b, MOX.** Top left triangle: Intra-  
611 sample  $\pi$  and symbiont fixation index ( $F_{ST}$ ) based on SNVs. Lower right triangle:  $\alpha$ - and  $\beta$ -  
612 diversity based on reconstructed strains. Rows and columns are labelled by sample name,  
613 sample location, and shell size. Heatmap hierarchical clustering is based on Euclidean distance  
614 of  $F_{ST}$ . **a, SOX:** mean pairwise  $F_{ST}$  is 0.618. Two subpopulations show an extreme degree of  
615 isolation: mean pairwise  $F_{ST}$  of subpopulation composed of M, N, R, is 0.313; mean pairwise  $F_{ST}$   
616 of subpopulation composed of L, O, P, Q is 0.308; mean  $F_{ST}$  of sample pairs where one sample  
617 is M, N, or R and the other sample is L, O, P, or Q is 0.969. **b, MOX:** mean pairwise  $F_{ST}$  is  
618 0.495. The clustering displays two groups: mean pairwise  $\beta$ -diversity of subpopulation  
619 composed of A, B, C, D, E, F, G, H, I, J, L is 0.099; mean pairwise  $\beta$ -diversity of subpopulation  
620 composed of K, M, N, O, P, Q, R, S is 0.383.

621





622

623 **Figure 3. Symbiont colonization dynamics.** **a**, The post larvae mussel gill does not take up  
 624 endosymbionts until the gill presents several filaments and the gill epithelial cells reach a  
 625 determined developmental stage<sup>26</sup>. At this time point, the filaments are simultaneously infected  
 626 by different strains via endocytosis (1). This imposes the first bottleneck in the symbiont  
 627 population, since most likely, not all the strains from the environmental pool can infect the  
 628 tissue. **b**, Bacteria are released from the host tissue to the environmental pool. As the mussel  
 629 grows, new filaments are continuously formed in the gill throughout the mussel life span  
 630 (growing cells shaded in purple). The new tissue is colonized by a self-infection process<sup>26</sup>,  
 631 which involves infection of the newly formed filaments via endocytosis with bacteria that are  
 632 released from old tissue via exocytosis (2). The spatial distribution of strains within the gill tissue  
 633 also supports self-infection<sup>45</sup>. The continuous self-infection process imposes serial founder  
 634 effects that lead to a reduction in strain diversity, which is mostly driven by drift. Additional  
 635 sources of diversity loss are: tissue replacement (3) and regulated lysosomal digestion of  
 636 symbionts<sup>58</sup> (4). **c**, In older mussels, a unique strain dominates the gill. In addition, *de novo*  
 637 mutations occur in symbiont genomes (marked by x). Due to serial founder effects within the  
 638 same mussel, those variants can be quickly fixed inside the mussel (5). **d**, As the mussel dies,  
 639 bacteria are released from the gill, going back to the environmental pool (6).

640

641

642 **Tables**

643 **Table 1. Neutrality index (NI) for the symbiont core genomes.**

644 **a**

	SOX		MOX	
	divergent	polymorphic	divergent	polymorphic
nonsynonymous SNVs	5004	990	2115	704
synonymous SNVs	10577	1450	1313	515
nonsynonymous SNVs/synonymous SNVs	0.47	0.68	1.61	1.37
NI	1.44		0.85	

645 **b**

	SOX		MOX	
	divergent	polymorphic	divergent	polymorphic
nonsynonymous SNVs	2549	3455	1041	1778
synonymous SNVs	6370	5657	649	1179
nonsynonymous SNVs/synonymous SNVs	0.40	0.61	1.60	1.51
NI	1.52		0.94	

646 **a**, divergent SNVs are all those SNVs that differ between at least two strains, i.e., all identified  
 647 strains are considered as diverged taxonomic units, and polymorphic SNVs are all the invariant  
 648 SNVs. **b**, Divergent SNVs have the same state inside a strain clade and are not invariant and  
 649 polymorphic SNVs are all the remaining, i.e., only the clades are considered as diverged  
 650 taxonomic units.

651

652 **Table 2. Nucleotide diversity ( $\pi$ ), Fixation Index ( $F_{ST}$ ), and pN/pS calculations for both**  
 653 **symbiont populations.**

	SOX	MOX
Intra-sample $\pi$ range	$5.2 \times 10^{-5}$ - $3.6 \times 10^{-3}$	$5.6 \times 10^{-6}$ - $7.0 \times 10^{-4}$
intra-sample $\pi$ mean	$1.4 \times 10^{-3} \pm 1.3 \times 10^{-3}$ (s.d)	$2.7 \times 10^{-4} \pm 2.8 \times 10^{-4}$ (s.d)
intra-sample $\pi$ median	$6.7 \times 10^{-4}$	$1.4 \times 10^{-4}$
Pairwise $F_{ST}$ range	0.151- 0.986	0.096- 0.898
Mean pairwise $F_{ST}$	0.618	0.495
pN/pS	0.137	0.425

654

- 656 1. McFall-Ngai, M. *et al.* Animals in a bacterial world, a new imperative for the life sciences. *Proc. Natl.*  
657 *Acad. Sci.* **110**, 3229–3236 (2013).
- 658 2. McFall-Ngai, M. J. The Importance of Microbes in Animal Development: Lessons from the Squid-  
659 *Vibrio* Symbiosis. *Annu. Rev. Microbiol.* **68**, 177–194 (2014).
- 660 3. Shabat, S. K. B. *et al.* Specific microbiome-dependent mechanisms underlie the energy harvest  
661 efficiency of ruminants. *Isme J.* **10**, 2958 (2016).
- 662 4. Schretter, C. E. *et al.* A gut microbial factor modulates locomotor behaviour in *Drosophila*. *Nature*  
663 **563**, 402–406 (2018).
- 664 5. Costello, E. K., Stagaman, K., Dethlefsen, L., Bohannan, B. J. M. & Relman, D. A. The Application of  
665 Ecological Theory Toward an Understanding of the Human Microbiome. *Science* **336**, 1255–1262  
666 (2012).
- 667 6. David, L. A. *et al.* Diet rapidly and reproducibly alters the human gut microbiome. *Nature* **505**, 559–  
668 563 (2014).
- 669 7. Sommer, F. *et al.* The Gut Microbiota Modulates Energy Metabolism in the Hibernating Brown Bear  
670 *Ursus arctos*. *Cell Rep.* **14**, 1655–1661 (2016).
- 671 8. Koren, O. *et al.* Host Remodeling of the Gut Microbiome and Metabolic Changes during Pregnancy.  
672 *Cell* **150**, 470–480 (2012).
- 673 9. Jones, R. J., Hoegh-Guldberg, O., Larkum, A. W. D. & Schreiber, U. Temperature-induced bleaching  
674 of corals begins with impairment of the CO<sub>2</sub> fixation mechanism in zooxanthellae. *Plant Cell Environ.*  
675 **21**, 1219–1230 (1998).
- 676 10. Riou, V. *et al.* Influence of CH<sub>4</sub> and H<sub>2</sub>S availability on symbiont distribution, carbon assimilation and  
677 transfer in the dual symbiotic vent mussel *Bathymodiolus azoricus*. *Biogeosciences* **5**, 1681–1691  
678 (2008).
- 679 11. Bright, M. & Bulgheresi, S. A complex journey: transmission of microbial symbionts. *Nat. Rev.*  
680 *Microbiol.* **8**, 218–30 (2010).
- 681 12. Wernegreen, J. J. Endosymbiont evolution: predictions from theory and surprises from genomes:  
682 Endosymbiont genome evolution. *Ann. N. Y. Acad. Sci.* **1360**, 16–35 (2015).
- 683 13. Woyke, T. *et al.* One Bacterial Cell, One Complete Genome. *PLoS ONE* **5**, e10314 (2010).
- 684 14. Guyomar, C. *et al.* Multi-scale characterization of symbiont diversity in the pea aphid complex  
685 through metagenomic approaches. *Microbiome* **6**, 181 (2018).
- 686 15. Boscaro, V. *et al.* Parallel genome reduction in symbionts descended from closely related free-living  
687 bacteria. *Nat. Ecol. Evol.* **1**, 1160 (2017).
- 688 16. Klose, J. *et al.* Endosymbionts escape dead hydrothermal vent tubeworms to enrich the free-living  
689 population. **112**, 11300–11305 (2015).
- 690 17. Hagen, M. J. & Hamrick, J. L. Population level processes in *Rhizobium leguminosarum* bv. *trifolii*: the  
691 role of founder effects. *Mol. Ecol.* **5**, 707–714 (1996).
- 692 18. Vega, N. M. & Gore, J. Stochastic assembly produces heterogeneous communities in the  
693 *Caenorhabditis elegans* intestine. *PLOS Biol.* **15**, e2000633 (2017).
- 694 19. Schloissnig, S. *et al.* Genomic variation landscape of the human gut microbiome. *Nature* **493**, 45–50  
695 (2013).
- 696 20. Ellegaard, K. M. & Engel, P. Genomic diversity landscape of the honey bee gut microbiota. *Nat.*  
697 *Commun.* **10**, 446 (2019).
- 698 21. Wollenberg, M. S. & Ruby, E. G. Population Structure of *Vibrio fischeri* within the Light Organs of  
699 *Euprymna scolopes* Squid from Two Oahu (Hawaii) Populations. *Appl. Environ. Microbiol.* **75**, 193–  
700 202 (2009).
- 701 22. Won, Y.-J. *et al.* Environmental Acquisition of Thiotrophic Endosymbionts by Deep-Sea Mussels of  
702 the Genus *Bathymodiolus*. *Appl. Environ. Microbiol.* **69**, 6785–6792 (2003).
- 703 23. Dubilier, N., Windoffer, R. & Giere, O. Ultrastructure and stable carbon isotope composition of the  
704 hydrothermal vent mussels *Bathymodiolus brevior* and *B. sp. affinis brevior* from the North Fiji Basin,  
705 western Pacific. *Mar. Ecol. Prog. Ser.* **165**, 187–193 (1998).
- 706 24. Duperron, S. *et al.* Diversity, relative abundance and metabolic potential of bacterial endosymbionts  
707 in three *Bathymodiolus* mussel species from cold seeps in the Gulf of Mexico. *Environ. Microbiol.* **9**,  
708 1423–1438 (2007).

- 709 25. Ansorge, R. *et al.* Diversity matters: Deep-sea mussels harbor multiple symbiont strains. *bioRxiv*  
710 531459 (2019).
- 711 26. Wentrup, C., Wendeberg, A., Schimak, M., Borowski, C. & Dubilier, N. Forever competent: Deep-sea  
712 bivalves are colonized by their chemosynthetic symbionts throughout their lifetime. *Environ.*  
713 *Microbiol.* **16**, 3699–3713 (2014).
- 714 27. Schöne, B. R. & Giere, O. Growth increments and stable isotope variation in shells of the deep-sea  
715 hydrothermal vent bivalve mollusk *Bathymodiolus brevior* from the North Fiji Basin, Pacific Ocean.  
716 *Deep Sea Res. Part Oceanogr. Res. Pap.* **52**, 1896–1910 (2005).
- 717 28. Van Dover, C. Community structure of mussel beds at deep-sea hydrothermal vents. *Mar. Ecol. Prog.*  
718 *Ser.* **230**, 137–158 (2002).
- 719 29. Nielsen, H. B. *et al.* Identification and assembly of genomes and genetic elements in complex  
720 metagenomic samples without using reference genomes. *Nat. Biotechnol.* **32**, 822–828 (2014).
- 721 30. Riou, V. *et al.* Influence of CH<sub>4</sub> and H<sub>2</sub>S availability on symbiont distribution, carbon assimilation and  
722 transfer in the dual symbiotic vent mussel *Bathymodiolus azoricus*. *Biogeosciences* **5**, 1681–1691  
723 (2008).
- 724 31. Shapiro, B. J. & Polz, M. F. Ordering microbial diversity into ecologically and genetically cohesive  
725 units. *Trends Microbiol.* **22**, 235–247 (2014).
- 726 32. Kashtan, N. *et al.* Single-cell genomics reveals hundreds of coexisting subpopulations in wild  
727 *Prochlorococcus*. *Science* **344**, 416–20 (2014).
- 728 33. Quince, C. *et al.* DESMAN: a new tool for de novo extraction of strains from metagenomes. *Genome*  
729 *Biol.* **18**, 181 (2017).
- 730 34. Ho, P.-T. *et al.* Geographical structure of endosymbiotic bacteria hosted by *Bathymodiolus* mussels  
731 at eastern Pacific hydrothermal vents. *BMC Evol. Biol.* **17**, 121 (2017).
- 732 35. Rocha, E. P. C. *et al.* Comparisons of dN/dS are time dependent for closely related bacterial  
733 genomes. *J. Theor. Biol.* **239**, 226–235 (2006).
- 734 36. Kryazhimskiy, S. & Plotkin, J. B. The population genetics of dN/dS. *PLoS Genet.* **4**, e1000304 (2008).
- 735 37. Rand, D. M. & Kann, L. M. Excess amino acid polymorphism in mitochondrial DNA: contrasts among  
736 genes from *Drosophila*, mice, and humans. *Mol. Biol. Evol.* **13**, 735–748 (1996).
- 737 38. Lorion, J. *et al.* Adaptive radiation of chemosymbiotic deep-sea mussels. *Proc R Soc B* **280**,  
738 20131243 (2013).
- 739 39. Achtman, M. & Wagner, M. Microbial diversity and the genetic nature of microbial species. *Nat. Rev.*  
740 *Microbiol.* **6**, 431–440 (2008).
- 741 40. Russell, S. L., Corbett-Detig, R. B. & Cavanaugh, C. M. Mixed transmission modes and dynamic  
742 genome evolution in an obligate animal–bacterial symbiosis. *ISME J.* **11**, 1359–1371 (2017).
- 743 41. Sprockett, D., Fukami, T. & Relman, D. A. Role of priority effects in the early-life assembly of the gut  
744 microbiota. *Nat. Rev. Gastroenterol. Hepatol.* **15**, 197–205 (2018).
- 745 42. Benson, A. K. *et al.* Individuality in gut microbiota composition is a complex polygenic trait shaped by  
746 multiple environmental and host genetic factors. *Proc. Natl. Acad. Sci.* **107**, 18933–18938 (2010).
- 747 43. Rothschild, D. *et al.* Environment dominates over host genetics in shaping human gut microbiota.  
748 *Nature* **555**, 210–215 (2018).
- 749 44. Wentrup, C., Wendeberg, A., Huang, J. Y., Borowski, C. & Dubilier, N. Shift from widespread  
750 symbiont infection of host tissues to specific colonization of gills in juvenile deep-sea mussels. *ISME*  
751 *J.* **7**, 1244–7 (2013).
- 752 45. Ikuta, T. *et al.* Heterogeneous composition of key metabolic gene clusters in a vent mussel symbiont  
753 population. *ISME J.* **10**, 990–1001 (2016).
- 754 46. Fontanez, K. M. & Cavanaugh, C. M. Evidence for horizontal transmission from multilocus phylogeny  
755 of deep-sea mussel (Mytilidae) symbionts. *Environ. Microbiol.* **16**, 3608–3621 (2014).
- 756 47. Ponnudurai, R. *et al.* Metabolic and physiological interdependencies in the *Bathymodiolus azoricus*  
757 symbiosis. *ISME J.* **11**, 463–477 (2017).
- 758 48. Reuter, M., Pedersen, J. S. & Keller, L. Loss of *Wolbachia* infection during colonisation in the  
759 invasive Argentine ant *Linepithema humile*. *Heredity* **94**, 364–369 (2005).
- 760 49. Didelot, X., Walker, A. S., Peto, T. E., Crook, D. W. & Wilson, D. J. Within-host evolution of bacterial  
761 pathogens. *Nat. Rev. Microbiol.* **14**, 150–162 (2016).
- 762 50. Gonzalez, R. J., Lane, M. C., Wagner, N. J., Weening, E. H. & Miller, V. L. Dissemination of a Highly  
763 Virulent Pathogen: Tracking The Early Events That Define Infection. *PLOS Pathog.* **11**, e1004587  
764 (2015).

765 51. Zhang, T. *et al.* Deciphering the landscape of host barriers to *Listeria monocytogenes* infection. *Proc.*  
766 *Natl. Acad. Sci. U. S. A.* **114**, 6334–6339 (2017).

767 52. Zhou, J., Bruns, M. A. & Tiedje, J. M. DNA Recovery from Soils of Diverse Composition. *Appl.*  
768 *Environ. Microbiol.* **62**, 316–322 (1996).

769 53. Bushnell, Brian. BMap. (2014). Available at: [sourceforge.net/projects/bbmap/](https://sourceforge.net/projects/bbmap/).

770 54. Nurk, S., Meleshko, D., Korobeynikov, A. & Pevzner, P. A. metaSPAdes: a new versatile  
771 metagenomic assembler. *Genome Res.* **27**, 824–834 (2017).

772 55. Hyatt, D., Locascio, P. F., Hauser, L. J. & Uberbacher, E. C. Gene and translation initiation site  
773 prediction in metagenomic sequences. *Bioinformatics* **28**, 2223–2230 (2012).

774 56. Kent, W. J. BLAT — The BLAST -Like Alignment Tool. *Genome Res.* **12**, 656–664 (2002).

775 57. Buchfink, B., Xie, C. & Huson, D. H. Fast and sensitive protein alignment using DIAMOND. *Nat.*  
776 *Methods* **12**, 59–60 (2015).

777 58. Sun, J. *et al.* Adaptation to deep-sea chemosynthetic environments as revealed by mussel genomes.  
778 *Nat. Ecol. Evol.* **1**, 0121 (2017).

779 59. Li, H. & Durbin, R. Fast and accurate short read alignment with Burrows-Wheeler transform.  
780 *Bioinformatics* **25**, 1754–1760 (2009).

781 60. Li, H. *et al.* The Sequence Alignment/Map format and SAMtools. *Bioinformatics* **25**, 2078–2079  
782 (2009).

783 61. Parks, D. H., Imelfort, M., Skennerton, C. T., Hugenholtz, P. & Tyson, G. W. CheckM: assessing the  
784 quality of microbial genomes recovered from isolates, single cells, and metagenomes. *Genome Res.*  
785 **25**, 1043–1055 (2015).

786 62. Subramanian, S. The effects of sample size on population genomic analyses – implications for the  
787 tests of neutrality. *BMC Genomics* **17**, 123 (2016).

788 63. Wilm, A. *et al.* LoFreq: A sequence-quality aware, ultra-sensitive variant caller for uncovering cell-  
789 population heterogeneity from high-throughput sequencing datasets. *Nucleic Acids Res.* **40**, 11189–  
790 11201 (2012).

791 64. Broad Institute. Best practices for variant calling with the GATK,  
792 <https://www.broadinstitute.org/partnerships/education/broade/best-practices-variant-calling-gatk-1>.

793 65. Huson, D. H. SplitsTree: analyzing and visualizing evolutionary data. *Bioinformatics* **14**, 68–73  
794 (1998).

795 66. Tria, F. D. K., Landan, G. & Dagan, T. Phylogenetic rooting using minimal ancestor deviation. *Nat.*  
796 *Ecol. Amp Evol.* **1**, 0193 (2017).

797 67. Nguyen, L.-T., Schmidt, H. A., von Haeseler, A. & Minh, B. Q. IQ-TREE: A Fast and Effective  
798 Stochastic Algorithm for Estimating Maximum-Likelihood Phylogenies. *Mol. Biol. Evol.* **32**, 268–274  
799 (2015).

800 68. Helmus, M. R., Bland, T. J., Williams, C. K. & Ives, A. R. Phylogenetic Measures of Biodiversity. *Am.*  
801 *Nat.* **169**, E68–E83 (2007).

802 69. Kembel, S. W. *et al.* Picante: R tools for integrating phylogenies and ecology. *Bioinformatics* **26**,  
803 1463–1464 (2010).

804 70. Chen, J. GUniFrac: Generalized UniFrac Distances. (2018). Available at: [https://CRAN.R-](https://CRAN.R-project.org/package=GUniFrac)  
805 [project.org/package=GUniFrac](https://CRAN.R-project.org/package=GUniFrac).

806 71. Stoletzki, N. & Eyre-Walker, A. The Positive Correlation between dN/dS and dS in Mammals Is Due  
807 to Runs of Adjacent Substitutions. *Mol. Biol. Evol.* **28**, 1371–1380 (2011).

808 72. R Core Team. *R: A Language and Environment for Statistical Computing*. (R Foundation for  
809 Statistical Computing, 2017).

810

811